RSC Advances

PAPER

View Article Online
View Journal | View Issue

Cite this: *RSC Adv.*, 2019, **9**, 12404

Fabrication and excellent electroresponsive properties of ideal PMMA@$BaTiO_3$ composite particles

Wen Liu,[ab] Zunyuan Xie,*[ab] Yaping Lu,[ab] Meixiang Gao,[c] Weiqiang Zhang [ab] and Lingxiang Gao *[ab]

A series of core–shell-structured poly(methylmethacrylate)@$BaTiO_3$ (PMMA@BT) composite particles were constructed *via* the self-assembly of BT nanoparticles on the surfaces of PMMA cores through the covalent bonding of siloxane groups at room temperature. The PMMA@BT composite particles were characterized by scanning electron microscopy, transmission electron microscopy, infrared spectroscopy, X-ray diffraction, video-based optical contact angle measurement, thermogravimetric analysis, and impedance analysis. The electroresponses of the obtained PMMA@BT composite particles were all stronger than that of pure BT, and the electroresponse depended on the weight percentage of the BT shell. The PMMA@BT particles with the optimal core–shell structure contained 58.14 wt% of BT shell. The surface hydrophilicity of the optimal particles was close to that of pure BT, and the dielectric constant was the greatest among the series of synthesized PMMA@BT particles. Thus, the optimized PMMA@BT particles demonstrated the strongest electroresponsive behavior in gelatin hydrogel elastomer, as demonstrated by polarized microscopy and dynamic mechanical analysis. The excellent electroresponsive property of the optimal PMMA@BT particles is reflected by the large sensitivity of the increase in storage modulus for the gelatin hydrogel elastomer containing the composite particles (21% at E = 0.8 kV mm^{-1} and a particle loading of 1.0 wt%), far greater than that of pure BT particles (4.7%). Based on the sensitive electroresponsive properties, the PMMA@BT particles have potential applications as electroresponsive materials.

Received 15th February 2019
Accepted 30th March 2019

DOI: 10.1039/c9ra01174a

rsc.li/rsc-advances

1. Introduction

Stimuli-responsive materials have attracted considerable interest due to their potential usage in various devices in the mechanical, biomedical and robotic fields, such as sensors, dampers, actuators, switches, valves, artificial muscles, and controlled drug delivery systems.[1–5] Existing research mainly focuses on precisely controllable responses to external stimuli, including temperature, pH, light, and electric or magnetic fields.[6–9] Electroresponsive materials are mostly made up of electrically polarizable particles, which behave as electric dipoles that can be polarized and attract or repel each other to form solid-like chains in the presence of an external electric field, and this is reversibly controlled.[10,11]

$BaTiO_3$ (BT) is an ideal polarizable material that is widely used because of its good chemical stability, thermo-stability and dielectric property.[12,13] In a certain electric field, BT can be spontaneously polarized, and the polarization direction can be parallel with the direction of the electric field. However, the high rigidity and density of BT induces serious sedimentation, hindering its response to the external electric field. To overcome these shortcomings, a number of attempts have been made to adjust the size and shape of BT, and particularly to modify its surface.[14–16] The incorporation of polymers into inorganic ceramics can improve the density, flexibility and dispersion stability of composite materials.[17,18] In addition, dielectric BT nanoparticles were attached onto the surface of the insulating polymer PVDF *via* hydrogen bonding between the two components. The novel composites were investigated as high-energy-density capacitor materials and achieved high dielectric constant and low dielectric loss.[19]

Previous studies found that BT@polymer particles with core–shell structures can be fabricated using surface-initiated polymers to improve the electroresponse of BT.[20–22] However, the polymers coated on the surface of BT clearly weakened the responsive effect of BT. Subsequently, Wang *et al.*[23] reported the preparation of gelatin@BT composite microspheres and

[a]*Key Laboratory of Applied Surface and Colloid Chemistry (Shaanxi Normal University), Ministry of Education, Xi'an, 710119, PR China. E-mail: gaolx@snnu.edu.cn; zyxie123@snnu.edu.cn; Fax: +86-29-8153-0727; Tel: +86-29-8153-0730; +86-29-81530813*

[b]*School of Chemistry & Chemical Engineering, Shaanxi Normal University, Xi'an 710119, PR China*

[c]*Yulin Vocational and Technical College, Yulin 719000, PR China*

studied their electroresponsive property in hydrogel elastomers. The electroresponse of BT particles has been improved to a great extent by adhering BT to a gelatin core. However, the improvement is insufficient due to the light weight of the BT shell and the inhomogeneous size of the microspheres. Based on the above research achievements, we continued to investigate approaches to promote the electroresponse of BT particles based on the "BT-shell" optimal effect.

PMMA is a long, soft chain of polymer compounds that has been widely used in many fields because of useful characters, such as good chemical stability, outstanding biocompatibility, non-toxicity, environmental friendliness, low cost, low density and transparent optical property.[24] PMMA is the primary choice for the preparation of polymer@BT composite particles due to its desirable properties. In this study, we fabricate PMMA@BT composite particles with six different BT shell weights and then disperse the particles in hydrogel elastomers cured with or without an applied electric field. After testing the storage moduli of the elastomers, the effect of the BT shell weight on the electroresponse of the composite particles was investigated.

2. Experimental

2.1. Materials

Sodium dodecyl benzene sulfonate (SDBS, $C_{18}H_{29}NaO_3S$) and methylmethacrylate monomers (MMA, $CH_2{=}CH(CH_3)COOCH_3$) were purchased from Tianjin Fuchen Chemical Reagent. Ethanol (C_2H_5OH) was purchased from Sinopharm Group Chemical Reagent. Potassium peroxydisulfate ($K_2S_2O_8$) was supplied by Aladdin Chemical Reagent. The four reagents were used as the surfactant, polymer monomers, solvent and initiator to prepare PMMA microspheres *via* emulsion polymerization.[25,26] γ-Methacryloxypropyltrimethoxysilane (KH570, $C_{10}H_{20}O_5Si$) was purchased from Aladdin Chemical Reagent and used as a surface modification agent. Methylglycol ($CH_3OCH_2CH_2OH$) and sodium hydroxide (NaOH) were supplied by Tianjin Fuchen and Sinopharm Group Chemical Reagent and used as the solvent and alkaline environment regulator, respectively. Barium hydroxide ($Ba(OH)_2\cdot 8H_2O$) was obtained from Sinopharm Group Chemical Reagent, and titanium tetrachloride ($TiCl_4$) was purchased from Shanghai Macklin Biochemical Co. Ltd. They were used as the raw materials to prepare BT particles *via* solvothermal synthesis. Hydrochloric acid (HCl) was purchased from Sinopharm Group and used as a pH regulator to prepare PMMA@BT composite particles *via* self-assembly deposition. Gelatin, glycerol ($C_3H_8O_3$) and glutaraldehyde ($C_5H_8O_2$) were obtained from Aladdin, Sinopharm Group Chemical Reagent and Tianjin Fuchen, respectively. They were used to prepare the particles/glycerin/gelatin composite hydrogel elastomers; gelatin acted as a polymer matrix, glycerol was a stabilizer, and glutaraldehyde was the cross-linking agent. All chemicals used in this experiment were of analytical grade and used without further purification. The water used in this work was purified by a water purification system (Qianyan Technology).

2.2. Preparation of PMMA@BT composite particles

2.2.1. Synthesis of PMMA particles. Typically, 0.2 g SDBS was added into a mixture of 30 mL anhydrous ethanol and 70 mL water in a 250 mL reaction container. The mixture was stirred for 40 min at 70 °C to dissolve SDBS completely. MMA (10 mL) was added into the mixture followed by continuous stirring for approximately 1 h. $K_2S_2O_8$ solution (10 mL, 0.037 mol L^{-1}) was then added under nitrogen protection. The polymerization was initiated and proceeded for 30 min until a white precipitate appeared, and the suspension was then stirred rapidly for approximately 10 h. Finally, the precipitate was centrifuged and washed several times with ethanol and water in turn and then dried in a vacuum oven at 60 °C. PMMA spheres with diameters of ~600 nm were obtained and used as the core material for subsequent syntheses.

2.2.2. Modification of PMMA with KH570. First, PMMA microspheres (0.5 g) were dispersed ultrasonically in 30 mL ethanol and stirred to form a stable and homogenous suspension. Second, KH570 (0.2 mL) was added to the suspension followed by stirring for 3 h at room temperature. The modified PMMA microspheres were filtered, washed with ethanol, and dried in a vacuum oven at a constant temperature. The resulting mono-dispersed PMMA microspheres were modified with silane coupling agent KH570, and reactive groups were introduced.

2.2.3. Synthesis of BT nanoparticles. The BT nanoparticles (NPs) were prepared by using a solvothermal synthesis method.[27] First, 1 mL of $TiCl_4$ was added drop-wise into 14 mL of absolute ethanol to form a clear yellow solution, named solution A. Second, 3.44 g of $Ba(OH)_2\cdot 8H_2O$ (Ba/Ti mol ratio = 1.2) was dissolved in 14 mL of $CH_3OCH_2CH_2OH$; this solution was named solution B. Subsequently, solution A was dropped into solution B under stirring for 30 min. Next, water was dropped into the mixture solution by keeping the total volume of the mixed solvent as 80 mL. Finally, 5.0 g NaOH was added under rapid stirring. The resulting suspension was subsequently transferred to a Teflon-lined stainless-steel autoclave. The autoclave was sealed, heated to 160 °C, and kept at this temperature for 24 h. After reaction completion, the reaction suspension was cooled naturally to room temperature, filtered, washed several times to neutral with water and absolute ethanol, and dried in an oven at 100 °C for 24 h. BT NPs with diameters of ~50 nm were obtained.

2.2.4. Attaching BT to PMMA (PMMA@BT composite particles). The PMMA@BT composite particles were prepared *via* self-assembly. Modified PMMA (0.1 g) was dispersed ultrasonically in 30 mL of mixed solvent (ethanol/water with a 1 : 2 volume ratio) to form a stable and homogenous suspension (suspension A). BT NPs were dispersed ultrasonically in ethanol to form a stable and homogenous suspension (suspension B). Subsequently, HCl solution (0.1 mol L^{-1}) was quickly injected into the mixed suspension of A and B followed by vigorous stirring to adjust the suspension pH to 2.8–3.0. The resulting suspension was stirred for another 3.5 h at room temperature. The precipitates were washed several times with ethanol and then dried in a vacuum oven for 10 h at 60 °C. Composite

particles with different BT contents (PMMA@BT-1 to PMMA@BT-6) were fabricated by controlling the mass ratio of PMMA to BT from 1 : 0.5 (PMMA@BT-1) to 1 : 3 (PMMA@BT-6; Table 1).[28–30]

2.3. Structural characterization

The morphologies of the products were examined by field-emission scanning electron microscopy (FESEM; SU-8020) and transmission electron microscopy (TEM; JEM-2100). The TEM samples were prepared by drying a drop of the ethanol suspension on a carbon-coated copper TEM grid. The structures of the particles were further characterized by Fourier transform infrared spectroscopy (FTIR; Tensor-27). Each particle was loaded in a KBr pellet and scanned over the wave number range of 4000 to 400 cm^{-1}. The crystal structure was determined by X-ray diffraction (XRD; DX-2700). Diffraction data were collected in the range of $2\theta = 10–70^\circ$ at a resolution of 0.05° per step with 6 s of integration time per step. The thermal stability of the series of PMMA@BT composite particles was studied by thermogravimetric analysis (TGA; Q-50). The samples were heated from 25 °C to 800 °C with a heating rate of 20 °C min^{-1}. Static water contact angles (CAs) were measured using the sessile drop method with a OCA20 video-based optical CA measuring apparatus. The testing process was as follows. Particles (2.0 wt%) were ultrasonically dispersed in ethanol to form a uniform suspension. A glass slide ($74 \times 25 \times 1.2$ mm^3) was immersed vertically in the ethanol suspension and then drawn out of the suspension at a low, constant speed. The slide was then allowed to dry naturally at room temperature. The dip coating was repeated three times to ensure that the particles were well coated on the glass slide. The contact angle was measured 10 s after the water droplet was dropped on the particle-floor surface. Each angle reported is the average value from three tests.

2.4. Property measurement

The relative dielectric properties of the particles were evaluated based on the dielectric constants of silicone oil suspensions in which the dried particles were dispersed with a volume fraction of 6% (η = 50 mPa s at 25 °C). The dielectric spectra of the suspensions were measured by an impedance analyzer (HP 4284A) in the frequency range of 20 Hz to 1 MHz using a measuring fixture (HP 16452A) for liquid. The main electro-responsive properties of the particles dispersed in hydrous elastomers were indirectly investigated by measuring the microstructures and storage modulus values of the hydrous composite elastomers *via* polarized microscopy and dynamic viscoelastic spectrometry (Q800DMA), respectively. The composite hydrous elastomers were prepared as follows. The particles (1.0 wt%) were dispersed uniformly in gelatin/glycerol/water mixture at 65 °C. Subsequently, a small amount of glutaraldehyde was quickly added into the mixture as the cross-linking agent, and the mixture was quickly transferred into two Plexiglas boxes ($40 \times 20 \times 8$ mm^3). Under the same conditions, the mixture in one box was cured under an external dc electric field ($E = 0.8$ kV mm^{-1}) for 50 min (kept at 65 °C for 30 min and then cooled naturally for 20 min). The mixture in the other box was not subjected to an electric field. The dc electric field was applied to one box in the upright direction at the beginning of the curing process with high-voltage power (regulator range = 0–30 kV; Tianjin Dongwen High Voltage Power Factory). The elastomer curing progress continued at room temperature for another 7 h without any applied field for each box. Finally, the particles/gelatin composite hydrous elastomers were prepared and named as follows: A-elastomers (cured without any electric field) and B-elastomers (cured under an 0.8 kV mm^{-1} electric field).[31,32] In general, the storage modulus (G) of elastomer was measured by Q800DMA under static-press multi-frequency mode in the frequency range of 1–10 Hz at room temperature. Each measurement was carried out and repeated at least five times. The difference in G between the A- and B-elastomers was explored to indirectly investigate the electroresponsive properties of the particles.

3. Results and discussion

3.1. Characterization of PMMA@BT particles

Fig. 1(a) schematically shows the synthetic process used to fabricate PMMA@BT composite particles. The six PMMA@BT particles with different BT contents were prepared by self-assembly (see Table 1).

3.1.1. Particle morphology. The SEM and TEM images of PMMA, modified PMMA, BT NPs and PMMA@BT-1–PMMA@BT-6 composite particles are shown in Fig. 2 and 3, respectively.

The bare PMMA particles had regular sizes of ~600 nm and were uniformly dispersed [Fig. 2(a)]. The PMMA particles were nearly mono-dispersed and had smooth surfaces, as shown in the TEM image in Fig. 3(a). Modified PMMA was coated with a slight layer of substance [Fig. 2(b) and 3(b)]. As shown in Fig. 2(c) and 3(c), the BT NPs had diameters of approximately 40–50 nm and were well dispersed.

When the BT NPs gathered on the PMMA surface, the surfaces of the composite particles were no longer smooth, and the average particle diameter increased gradually with increasing mass ratio of PMMA to BT [Fig. 2(d–i) and 3(d–i)]. The SEM and TEM images indicate that the PMMA@BT-1–PMMA@BT-6 particles all had PMMA@BT core–shell structures. Among them, the PMMA@BT-4 composite particle possessed the most perfect core–shell structure in which the BT NPs completely covered the surfaces of the PMMA spheres, and no free BT NPs were scattered.

Table 1 Different mass input ratios of the composite particles

m(PMMA) : m(BT)	1 : 0.5	1 : 1	1 : 1.5	1 : 2	1 : 2.5	1 : 3
PMMA@BT	PMMA@BT-1	PMMA@BT-2	PMMA@BT-3	PMMA@BT-4	PMMA@BT-5	PMMA@BT-6

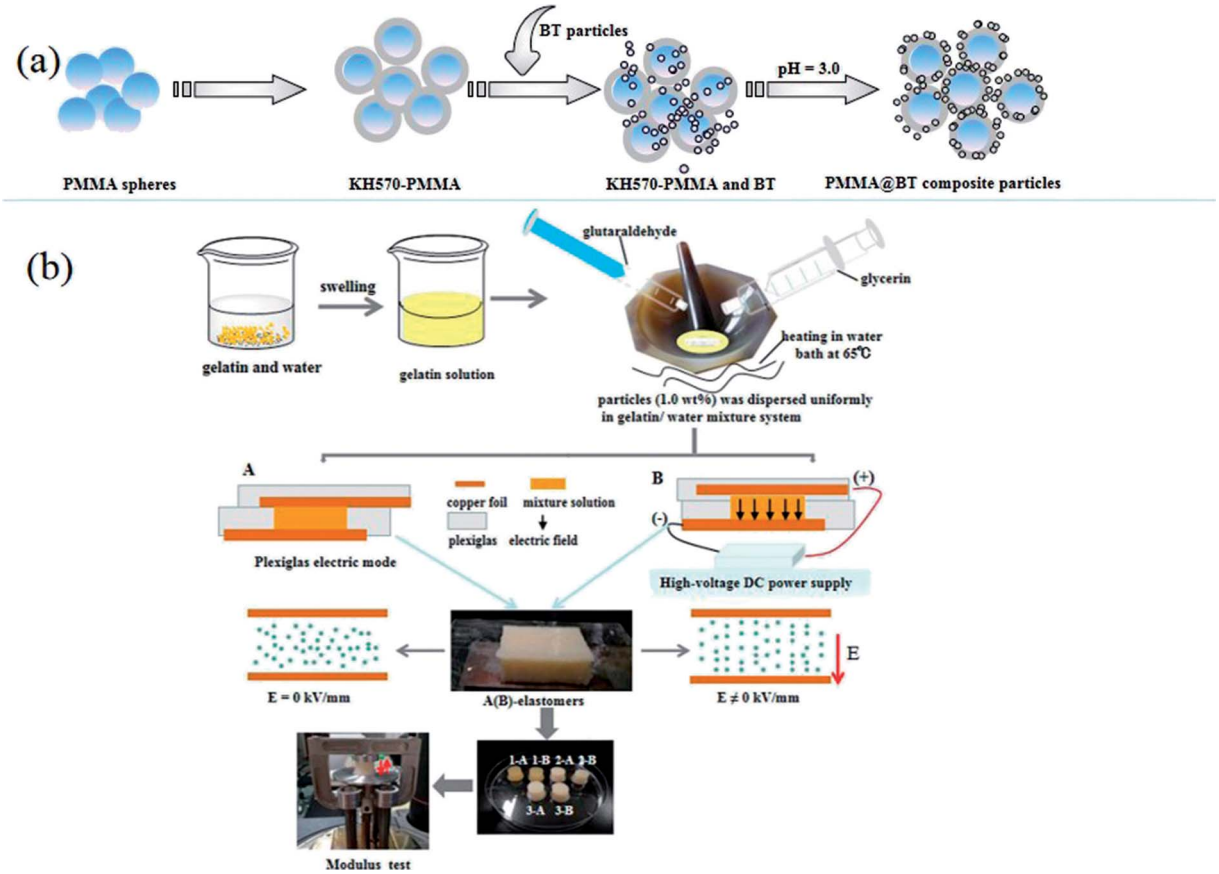

Fig. 1 (a) Graphical illustration of the synthetic process used to fabricate PMMA@BT particles. (b) Graphical illustration of the preparation of PMMA@BT/gelatin/water elastomers and measurement of their storage moduli.

3.1.2. Structure and content of particles. The FT-IR spectra of PMMA, modified PMMA, BT NPs, and PMMA@BT particles are shown in Fig. 4(1). Curve (a) in Fig. 4(1) shows the spectrum of PMMA. The sharp intense peak near 1730 cm^{-1} is attributed to ester carbonyl stretching vibrations; the peaks at 2996, 2952 and 2842 cm^{-1} belong to the C–H stretching vibration; and the peaks at 752 and 840 cm^{-1} are attributed to the puckering vibrations and deformation vibrations of O–C–O in PMMA, respectively. The peak at 3625 cm^{-1} arises from the –OH stretching of adsorbed light water. It should be noted that no peak is observed in the 1680–1640 cm^{-1} range, which confirms that all methyl methacrylate (MMA) monomer was polymerized into PMMA.[33] After PMMA was modified by KH570 [curve (b) in Fig. 4(1)], the peaks at 2996, 2952, 2842 and 1730 cm^{-1} were stronger than for PMMA owing to the combination of PMMA and KH570. The peak at 1076 cm^{-1}, which corresponds to C–O in PMMA, shifted to 1065 cm^{-1}, indicating the formation of C–O–Si. The stronger peak at 3625 cm^{-1} indicates that the $SiOCH_3$ group of KH570 develops into Si–OH after hydrolysis. We can conclude that the spectral changes were induced by the reaction between the coupling agent and PMMA.[34]

The KH570 coupling agent contains two chemical functional groups that can bond with the polymer molecules and inorganic material as a bridge. One group combines with PMMA materials to form strong interfacial bonds, and the other group reacts with the hydroxyl groups (–OH) of BT, forming covalent bonds through hydrolysis condensation, dehydration and solidification under certain conditions.[35,36] Fig. 4(1) curve (e) shows the characteristic peaks of BT at 1438 and 857 cm^{-1}; the peaks at 560 and 435 cm^{-1} correspond to fingerprint absorption. Moreover, the broad band centered at 3464 cm^{-1} is attributed to the hydroxyl stretching vibrations of BT. In contrast, in Fig. 4(1) curve (c), this band of BT–OH has shifted from 3464 to 3445 cm^{-1}, suggesting the dehydration of BT–OH and Si–OH and the generation of strong interactions between modified PMMA and BT.[37] Curves (c) and (d) are similar, confirming that BT and PMMA were attached *via* chemical bonds. Thus, under the action of the KH570 coupling agent, BT can be successfully assembled on the surface of PMMA.

Fig. 4(2) shows the XRD patterns of PMMA, modified PMMA, BT NPs and PMMA@BT-4 composite particles. In curve (a), the two characteristic wide diffraction bands at 15° and 30° partly belong to crystalline PMMA. After modification with KH570 [curve (b)], the characteristic diffraction bands of PMMA were visibly diminished, demonstrating that the surfaces of the PMMA microspheres were covered with amorphous KH570. In curve (c), the peaks are sharp and match well the standard pattern for BT (JCPDS no. 05-0626), suggesting high-purity BT NPs. One characteristic peak of BT ($2\theta = 44.5°$)[38] does not split, corresponding to its cubic phase. The XRD pattern of

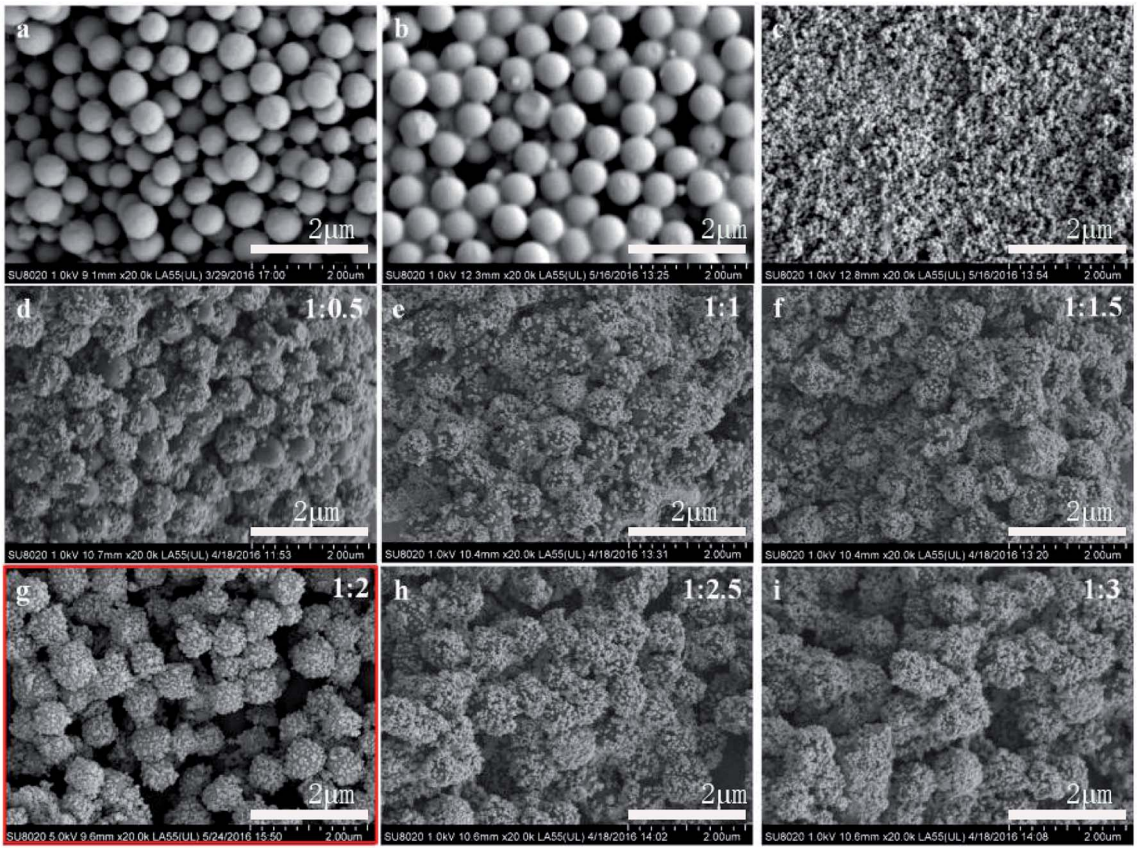

Fig. 2 SEM images of (a) pure PMMA spheres, (b) PMMA modified by KH570, (c) BT NPs, and (d–i) PMMA@BT-1–PMMA@BT-6 composite particles.

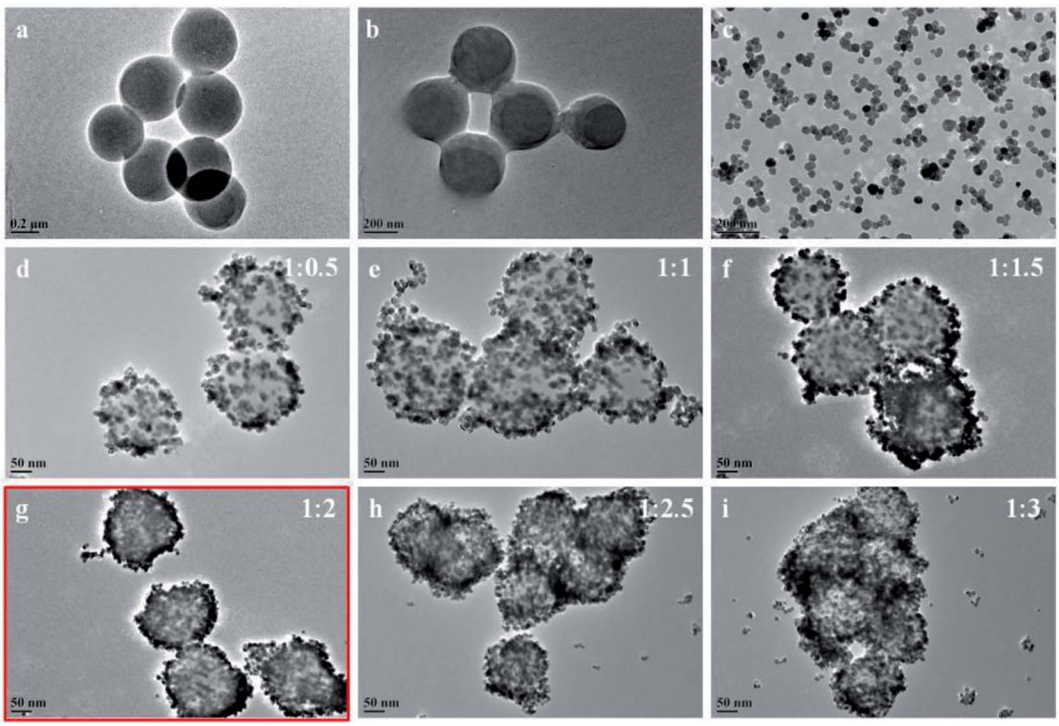

Fig. 3 TEM images of (a) pure PMMA spheres, (b) PMMA modified by KH570, (c) BT NPs, and (d–i) PMMA@BT-1–PMMA@BT-6 composite particles.

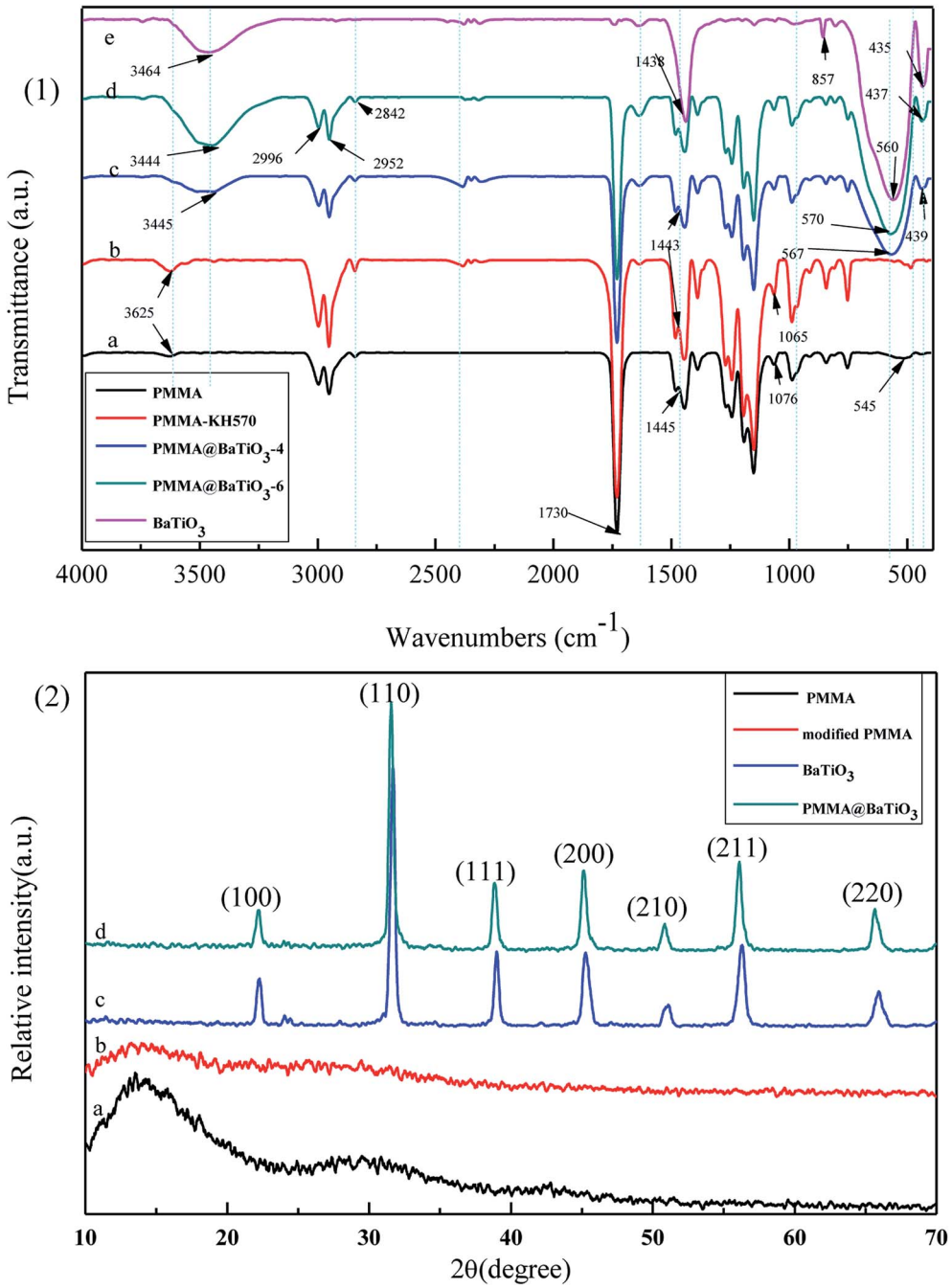

Fig. 4 (1) FT-IR spectra of pure PMMA (a), PMMA-KH570 (b), PMMA@BT-4 (c), PMMA@BT-6 (d), and BT NPs (e). (2) XRD spectra of pure PMMA (a), modified PMMA (b), BT NPs (c) and PMMA@BT-4 composite particles (d).

PMMA@BT is indicative of the typical cubic phase, similar to pure BT. This demonstrates that fine cubic structure of BT was retained during the assembly process.

TGA was conducted to calculate the amount of BT adhered to PMMA. As shown in Fig. 5, all curves except curve (b) indicate slight weight loss below 200 °C, corresponding to the release of the moisture and residual organic solvent entangled in the polymer chains. The significant weight loss at temperatures between 200 °C and 286 °C is attributed to the decomposition of oxygen-containing functional groups, while the sharp weight loss between 286 °C and 420 °C arises from degradation of the C–C chain skeleton of PMMA. Curve (b) shows almost no weight loss except for the release of the moisture, indicating that BT has good thermal stability.[39] However, the curves of the PMMA@BT composite particles with different BT contents [curves (c–h)] show two obvious weight losses at 200–360 °C and 360–420 °C, corresponding to the decomposition of oxygen-containing functional groups and the degradation of C–C chains, respectively. For the second stage of weight loss, the onset decomposition temperature remained the same, and the

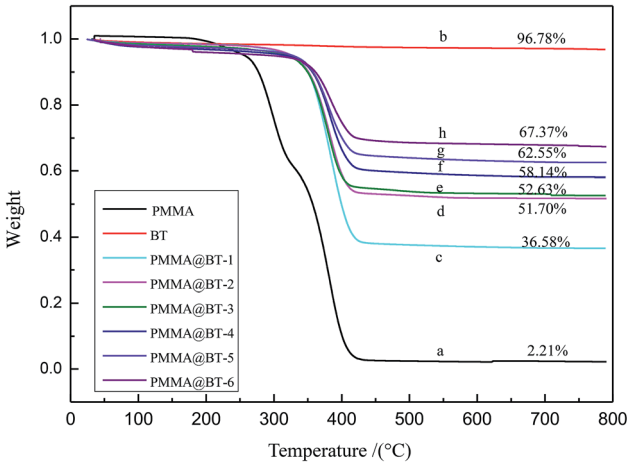

Fig. 5 TGA curves of PMMA (a), BT (b) and PMMA@BT-1–PMMA@BT-6 (c–h) composite particles.

final residues for the PMMA@BT composites gradually increased with increasing BT content .[40] The unchanged decomposition temperature is explained by two factors: the composites have the same chemical interaction between PMMA and BT, and BT has good thermal stability between the measured temperature region. Comparing curves (c–h) with curve (b) indicates that the final residue for the PMMA@BT composites is BT. Based on the mass percent of the final residue, the relative BT contents in the PMMA@BT composites (Φ_{BT}) were 36.56%, 51.70%, 52.63%, 58.14%, 62.55%, 67.37% from PMMA@BT-1 to PMMA@BT-6, respectively, close to the corresponding input mass percentages of BT.

3.2. Properties of PMMA@BT particles

3.2.1. Particle hydrophilicity. To compare the surface hydrophilic properties, the water CAs of PMMA, modified PMMA, BT, and PMMA@BT-1–PMMA@BT-6 composite particles were determined. As shown in Fig. 6(a–i), the water CAs of the samples increased in the following order: BT < PMMA@BT-6 ≈ PMMA@BT-5 ≈ PMMA@BT-4 < PMMA@BT-3 < PMMA@BT-2 < PMMA@BT-1 < modified PMMA < PMMA. The surface of the PMMA particle was hydrophobic, whereas the surface of the BT particle was super-hydrophilic.[32,34] The surfaces of the PMMA@BT composite particles were between hydrophobic and super hydrophilic, and the surface hydrophilicity gradually increased with BT content. This is attributed to the existence of a large number of –OH hydrophilic groups on the surfaces of the BT NPs. In the FT-IR spectrum of BT in Fig. 4(2), the strong, broad band centering at 3464 cm^{-1} is attributed to the hydroxyl stretching vibrations of BT, indicating that the BT NPs have a large number of hydrophilic –OH groups on the surface. However, this band is weaker in the FT-IR spectra of PMMA and modified PMMA, indicating that the PMMA and modified PMMA particles had fewer hydrophilic –OH groups on their surfaces. Therefore, when the content of BT NPs on PMMA increased, the surface hydrophilicity of the particles continuously increased.

3.2.2. Dielectric properties of particles. The relative dielectric constants (ε') of the silicone oil suspensions containing dispersed BT particles and PMMA@BT particles are shown in Fig. 7(A). The dielectric spectra of the suspensions reflect the contributions of silicone oil and dispersed particles. The dielectric constants decreased in the following order: ε'(BT) > ε'(PMMA@BT-4) > ε'(PMMA@BT-5) > ε'(PMMA@BT-6) > ε'(PMMA@BT-3) > ε'(PMMA@BT-2) > ε'(PMMA) > ε'(PMMA@BT-1). This is attributed to the lower ε' of the polymer PMMA compared to BT; thus, the dielectric constants of the PMMA@BT particles were lower than that of BT. Among the composite particles, PMMA@BT-4 had the highest ε'. This might be attributed to the high content of BT shell and the perfect surface structure of the particles, which combined to determine the interfacial polarization and ε'.[41,42]

3.2.3. Electroresponsive properties of the particles. To further explore the responsive performances of the elastomers filled with particles under an electric field, the sensitivity of the increase in storage modulus ($\Delta G/G_A$) of each elastomer was determined as follows:[46] $\Delta G = G_B - G_A$, $\Delta G/G_A = (G_B - G_A)/G_A$.

As shown in Fig. 7(B) and (C), $\Delta G/G_A \approx 0$ for the A and B elastomers containing dispersed pure PMMA particles (*e.g.*, Φ_{BT}

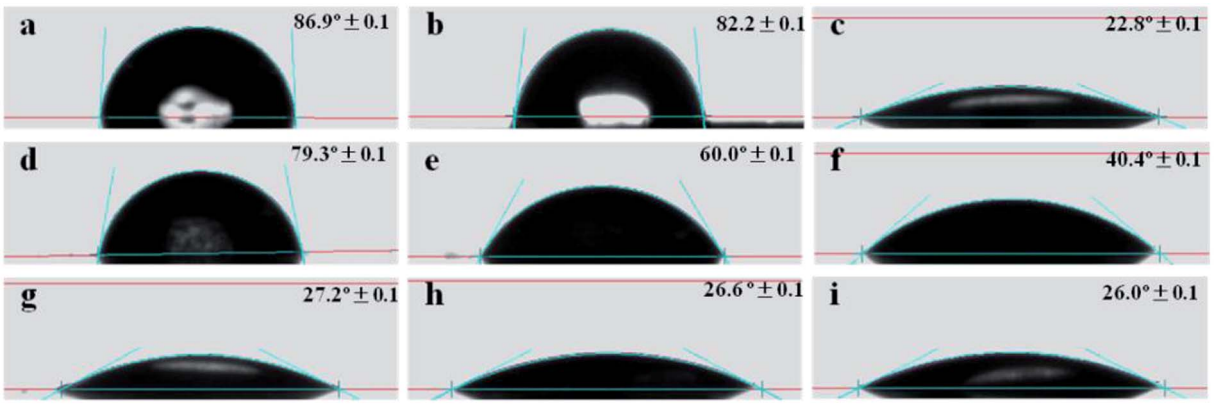

Fig. 6 Contact angles of water drops (3 μL) on the floors of PMMA (a), modified PMMA (b), BT (c) and (d–i) PMMA@BT-1–PMMA@BT-6 composite particles, respectively.

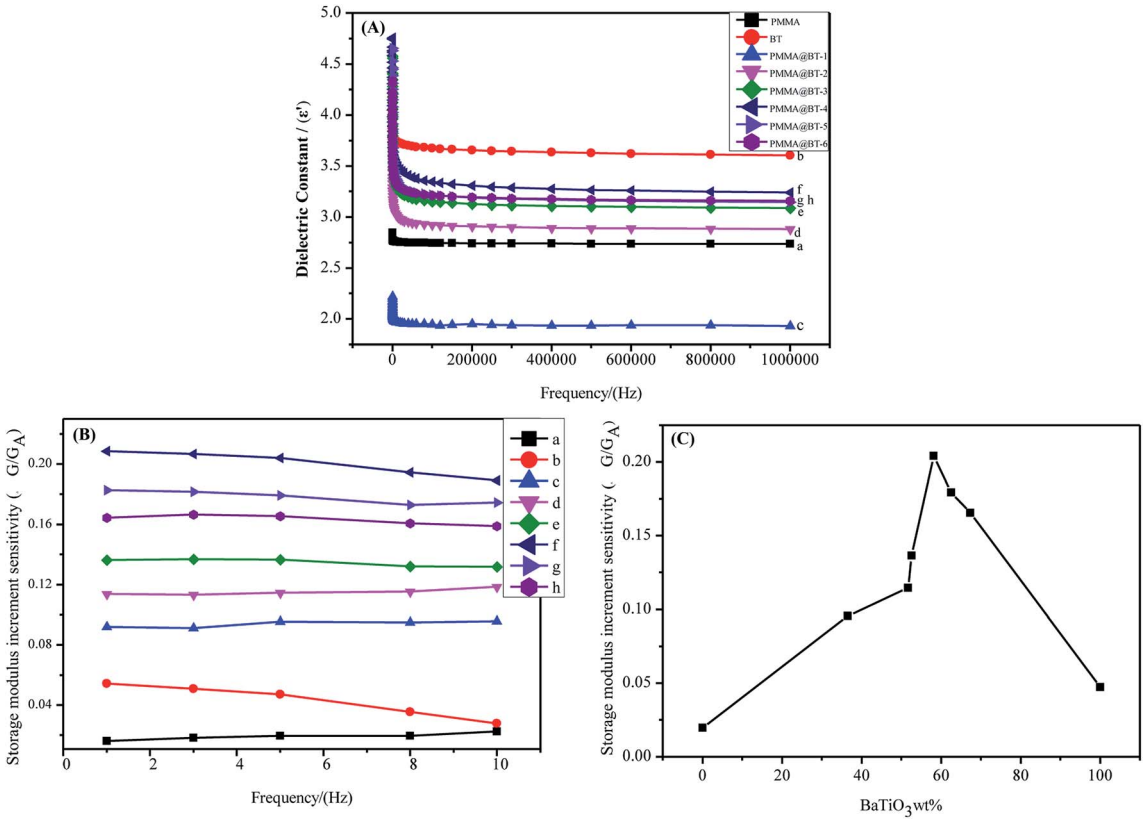

Fig. 7 (A) Dielectric constant of silicone oil suspensions containing dispersed PMMA (a), BT (b) and (c–h) PMMA@BT-1–PMMA@BT-6 particles, respectively. (B) Storage modulus increment sensitivity ($\Delta G/G_A$) *vs.* the frequency of elastomers filled with particles: (a) PMMA; (b) BT; and (c–h) PMMA@BT-1–6, respectively. (C) $\Delta G/G_A$ as a function of the wt% BT in the particles at a frequency of 5 Hz.

= 0). This suggests that the pure PMMA particles hardly responded to the applied electric field. The value of $\Delta G/G_A$ was much smaller for pure BT ($\Phi_{BT} = 1$), indicating that pure BT had a weak response to the electric field. This may be attributed to the large density and poor dispersion stability of BT in the elastomers. The six composite particles (PMMA@BT-1–PMMA@BT-6) exhibited positive responses to the electric field, as shown in Fig. 7(C).[43] As dielectric materials, BT and PMMA@BT particles can be polarized and induce positive/negative charges on the opposite sides of the particles. It is referred to induced dipoles. The attractive and repulsive interactions between the induced dipoles in the field direction cause the adjacent particles to attract or repel each other. Competition between the two kinds of electrostatic forces can cause the

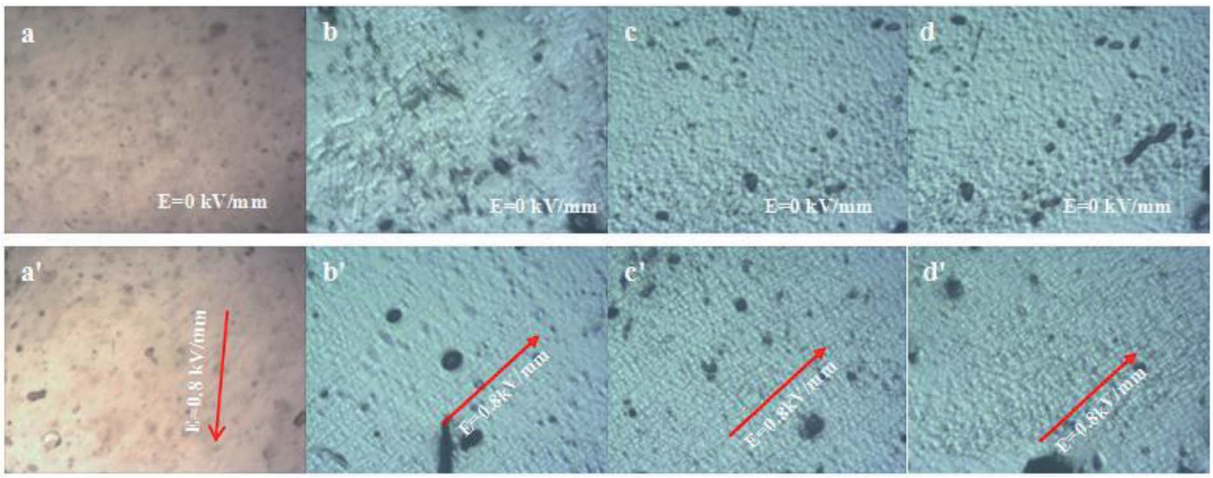

Fig. 8 Polarized microscope images of the sliced elastomers filled with particles with a mass fraction of 1.0 wt%: a(a')–d(d') PMMA, BT, PMMA@BT-4 and PMMA@BT-6, respectively; (a–d) and (a'–d') represent A and B elastomers, respectively.

particles to form chains and support elastomers in the field direction.[44,45] Therefore, the adjacent aligned particles in the B elastomers ($E = 0.8$ kV mm^{-1}) in the field direction could resist stress better than the randomly distributed particles in the A elastomers ($E = 0$ kV mm^{-1}). As a result, $\Delta G/G_A > 0$.

Plots of $\Delta G/G_A$ *versus* frequency are shown in Fig. 7(B). $\Delta G/G_A$ decreased in the following order: PMMA@BT-4 > PMMA@BT-5 > PMMA@BT-6 > PMMA@BT-3 > PMMA@BT-2 > PMMA@BT-1 > BT > PMMA. Thus, the electroresponses of the PMMA@BT composite particles were all are stronger than that of pure BT. Fig. 7(C) shows $\Delta G/G_A$ as a function of Φ_{BT} at the frequency of 5 Hz. $\Delta G/G_A$ first increased and then decreased with increasing Φ_{BT}. The largest $\Delta G/G_A$ (21%) occurred at $\Phi_{BT} \approx 58$ wt%. This can be explained by the excellent hydrophilic surface properties (Fig. 6), high dielectric constant [Fig. 7(A)], and fine dispersion (Fig. 9) of the PMMA@BT-4 ($\Phi_{BT} = 58.14$ wt%) particles. These properties make the PMMA@BT-4 compatible with hydrous media; thus, the particles are strongly polarized and form an excellent pearl-chain under an electric field.[47] When Φ_{BT} exceeded 58 wt%, the heavy BT particles resulted in heavy composite particles (PMMA@BT-5 and PMMA@BT-6), resulting in particle settlement in the aqueous elastomers, which weakened the chain effect. Hence, the PMMA@BT-4 composite particles possessed the strongest response to the electric field ($\Delta G/G_A = 21\%$).

The polarized microscope images of the sliced elastomers filled with the PMMA, BT, PMMA@BT-4 and PMMA@BT-6 particles are shown in Fig. 8. In Fig. 8(a) and (a′), the elastomers are filled by PMMA particles, but no ordered particle structure is observed in (a′). This indicates that PMMA hardly had a response to the applied electric field. In Fig. 8(b)–(d), BT and PMMA@BT particles are embedded in the elastomers and well isolated randomly in the A elastomers. Thus, the freely dispersed particles contribute a filling effect in the elastomers. Upon applying an electric field to B elastomers [Fig. 8(b′)–(d′)], the pearl-chain structures of BT and PMMA@BT particles were visibly aligned, especially for PMMA@BT-4. This result confirms the aforementioned electroresponses of BT and PMMA@BT particles along with the strongest response of the PMMA@BT-4 composite particles. This enhanced electroresponsive property of the PMMA@BT-4 composite particles may be explained by the dielectric property and dispersion of the particles. The higher dielectric constant of the particles facilitates a stronger "pearl chain" effect and strengthens the modulus of the corresponding B elastomer. The fine dispersion of the particles benefits the formation of "pearl chains" in the B elastomer and results in a larger difference in modulus between the A and B elastomers. The synergistic effect of the high dielectric constant and fine dispersion of the PMMA@BT-4 particles caused these particles to have the strongest response to the electric field.

Fig. 9 Suspensions of PMMA/$BaTiO_3$ and $BaTiO_3$ particles after sitting for 3 h.

4. Conclusions

This study demonstrates a facile approach to fabricate core–shell-structured PMMA@BT composite particles with different contents of BT shell by assembling BT nanoparticles onto PMMA cores *via* covalent bonds. Among the series of six synthesized composite particles, PMMA@BT-4 (58.14 wt% BT particles) exhibited the best core–shell structure, and the BT NPs were evenly distributed on the surface of PMMA. Importantly, the PMMA@BT composite particles had excellent dielectric properties and hydrophilic surfaces similar to pure BT. Meanwhile, the fine dispersity of the composite particles was superior to that of pure BT. As a result, the PMMA@BT composite particles exhibited strong responses to an electric field in hydrogel elastomers. The perfect assembly of BT on PMMA promoted the electroresponsive property of BT, resulting in an electroresponse quadruple that of BT under an 0.8 kV mm^{-1} electric field.

Appendix

Certain amounts of BT and PMMA@BT-4 particles were separately dispersed ultrasonically in water, forming two uniform suspensions with the same weight concentration of particles. After allowing to sit for 3 h, particle sedimentation was observed, as shown in the figure. The BT particles almost completely settled, whereas the PMMA@BT-4 particles only slightly settled. Thus, the dispersion of BT particles was greatly improved by anchoring on PMMA.

Conflicts of interest

There are no conflicts to declare. With the consent of all the authors, we made corrections.

Acknowledgements

This work was financially supported by the Fund for Graduate Innovation (No. 2018CSLY010) and the National Natural Science Foundation of China (No. 1203010328).

References

1 Y. D. Liu and H. J. Choi, Electrorheological Fluids: Smart Soft Matter and Characteristics, *Soft Matter*, 2012, **8**, 11961–11978.

2 L. C. Ho, C. H. Hsu, C. M. Ou, C. W. Wang, T. P. Liu, L. P. Hwang, Y. Y. Lin and H. T. Chang, Unibody core-shell smart polymer as a theranostic nanoparticle for drug delivery and MR imaging, *Biomaterials*, 2015, **37**, 436–446.

3 M. Mrlík, M. Ilčíková, T. Plachý, V. Pavlínek, Z. Špitalský and J. Mosnáček, Graphene oxide reduction during surface-initiated atom transfer radical polymerization of glycidyl methacrylate: Controlling electro-responsive properties, *Chem. Eng. J.*, 2016, **283**, 717–720.

4 W. L. Zhang, S. H. Piao and H. J. Choi, Facile and fast synthesis of polyaniline-coated poly(glycidyl methacrylate) core–shell microspheres and their electro-responsive characteristics, *J. Colloid Interface Sci.*, 2013, **402**, 100–106.

5 H. Y. Kim and H. J. Choi, Core–shell structured poly(2-ethylaniline) coated crosslinked poly(methyl methacrylate) nanoparticles by graft polymerization and their electrorheology, *RSC Adv.*, 2014, **4**, 28511–28518.

6 D. Roy, J. N. Cambre and B. S. Sumerlin, Future perspectives and recent advances in stimuli-responsive materials, *Prog. Polym. Sci.*, 2010, **35**, 278–301.

7 M. Karimi, A. Ghasemi, P. S. Zangabad, R. Rahighi, S. M. M. Basri, H. Mirshekari, M. Amiri, Z. S. Pishabad, A. Aslani, M. Bozorgomid, D. Ghosh, A. Beyzavi, A. Vaseghi, A. R. Aref, L. Haghani, S. Bahrami and M. R. Hamblin, Smart micro/nanoparticles in stimulus-responsive drug/gene delivery systems, *Chem. Soc. Rev.*, 2016, **45**, 1457–1501.

8 T. Manouras and M. Vamvakaki, Field responsive materials: photo-, electro-, magnetic- and ultrasound-sensitive polymers, *Polym. Chem.*, 2017, **8**, 74–96.

9 Y. F. Luo and X. H. Yu, Light and electrically responsive materials based on aligned carbon nanotubes, *Eur. Polym. J.*, 2016, **82**, 290–299.

10 T. Plachy, M. Sedlacik, V. Pavlinek, M. Trchová, Z. Morávková and J. Stejskal, Carbonization of aniline oligomers to electrically polarizable particles and their use in electrorheology, *Chem. Eng. J.*, 2014, **256**, 398–406.

11 J. B. Yin, X. Xia, X. X. Wang and X. P. Zhao, The electrorheological effect and dielectric properties of suspensions containing polyaniline@titania nanocable-like particles, *Soft Matter*, 2011, **7**, 10978–10986.

12 X. F. Su, B. C. Riggs, M. Tomozawa, J. K. Nelson and D. B. Chrisey, Preparation of $BaTiO_3$/low melting glass core–shell nanoparticles for energy storage capacitor applications, *J. Mater. Chem. A*, 2014, **2**, 18087–18096.

13 S. W. Kwon and D. H. Yoon, Effects of heat treatment and particle size on the tetragonality of nano-sized barium titanate powder, *Ceram. Int.*, 2007, **33**, 1357–1362.

14 H. Zhang, X. H. Wang, Z. B. Tian, C. F. Zhong, Y. C. Zhang, C. K. Sun and L. T. Li, Fabrication of Monodispersed 5-nm $BaTiO_3$ Nanocrystals with Narrow Size Distribution via One-Step Solvothermal Route, *J. Am. Ceram. Soc.*, 2011, **94**, 3220–3222.

15 Q. Ma, K. I. Mimura and K. Kato, Tuning shape of barium titanate nanocubes by combination of oleic acid/tert-butylamine through hydrothermal process, *J. Alloys Compd.*, 2016, **655**, 71–78.

16 M. Zhu, X. Y. Huang, K. Yang, X. Zhai, J. Zhang, J. L. He and P. K. Jiang, Energy Storage in Ferroelectric Polymer Nanocomposites Filled with Core-Shell Structured Polymer@$BaTiO_3$ Nanoparticles: Understanding the Role of Polymer Shells in the Interfacial Regions, *ACS Appl. Mater. Interfaces*, 2014, **6**, 19644–19654.

17 Y. Qiao, M. S. Islam, L. Wang, Y. Yan, J. Y. Zhang, B. C. Benicewicz, H. J. Ploehn and C. B. Tang, Thiophene Polymer-Grafted Barium Titanate Nanoparticles toward Nanodielectric Composites, *Chem. Mater.*, 2014, **26**, 5319–5326.

18 W. Choi, K. Choi, G. Yang, J. C. Kim and C. Yu, Improving piezoelectric performance of lead-free polymer composites with high aspect ratio BaTiO3 nanowires, *Polym. Test.*, 2016, **53**, 143–148.

19 M. F. Lina and P. S. Lee, Formation of PVDF-g-HEMA/$BaTiO_3$ nanocomposites via in situ nanoparticle synthesis for high performance capacitor applications, *J. Mater. Chem. A*, 2013, **1**, 14455–14459.

20 L. X. Gao, L. Li, X. R. Qi, W. X. Wei, J. L. Hai, W. Q. Gao and Z. W. Gao, Enhancement on Electric Responses of $BaTiO_3$ Particles with Polymer-Coating, *Polym. Compos.*, 2013, **14**, 897–903.

21 K. Hayashida, Y. Matsuoka and Y. Takatani, An ideal nanostructure of polymer/$BaTiO_3$ dielectric materials with high reliability for breakdown strength: isolated and uniformly dispersed $BaTiO_3$ nanoparticles by thick polymer shells, *RSC Adv.*, 2014, **4**, 33530–33536.

22 S. A. Paniagua, Y. Kim, K. Henry, R. Kumar, J. W. Perry and S. R. Marder, Surface-initiated polymerization from Barium Titanate Nanoparticles for Hybrid Dielectric Capacitors, *ACS Appl. Mater. Interfaces*, 2014, **6**, 3477–3482.

23 X. M. Wang, S. Xu and W. Q. Xu, Luminescent properties of dye–PMMA composite nanospheres, *Phys. Chem. Chem. Phys.*, 2011, **13**, 1560–1567.

24 X. L. Yang, Y. P. Lu, M. X. Gao, Z. Y. Xie and L. X. Gao, The preparation of Gelatin/$BaTiO_3$ core-shell composite particles and the electric field response performance, *J. Inorg. Mater.*, 2016, **31**, 1306–1310.

25 V. H. Pham, T. T. Dang, S. H. Hur, E. J. Kim and J. S. Chung, Highly Conductive Poly(methyl methacrylate) (PMMA)-Reduced Graphene Oxide Composite Prepared by Self-Assembly of PMMA Latex and Graphene Oxide through Electrostatic Interaction, *ACS Appl. Mater. Interfaces*, 2012, **4**, 2630–2636.

26 E. Kim, Y. Lee, J. Bang, K. Kim and S. Choe, Synthesis and electrical resistivity of the monodisperse PMMA/Ag hybrid particles, *Mater. Chem. Phys.*, 2012, **134**, 814–820.

27 K. S. Hong, M. G. Ha, J. S. Bae, J. S. Kim, Y. R. Bae, C. W. Ahn, I. W. Kim and J. P. Kim, Structural characteristics and chemical bonding states with temperature in barium titanate nanopowders prepared by using the solvothermal method, *Curr. Appl. Phys.*, 2015, **15**, 1377–1383.

28 Y. H. Min, Y. Fang, X. J. Huang, Y. H. Zhu, W. S. Li, J. M. Yuan, L. G. Tan, S. Y. Wang and Z. J. Wu, Surface modification of basalt with silane coupling agent on

asphalt mixture moisture damage, *Appl. Surf. Sci.*, 2015, **346**, 497–502.

29 S. L. Peng, J. H. Wei, J. Shi, Z. Y. Liu, W. F. Tang and W. J. Wen, The Synthesis and Electrorheological Properties of $BaTiO_3$-coated PMMA Microspheres, *J. Wuhan Univ. Technol., Mater. Sci. Ed.*, 2007, **22**, 85–87.

30 S. Guo, S. X. Zhou, H. J. Li and B. You, Light diffusing films fabricated by strawberry-like PMMA/SiO_2 composite microspheres for LED application, *J. Colloid Interface Sci.*, 2015, **448**, 123–129.

31 L. X. Gao and X. P. Zhao, Mechanical and Electrical Properties of Hydrous Electrorheological Elastomers Based on Gelatin/Glycerin/Water Hybrid, *J. Appl. Polym. Sci.*, 2007, **104**, 1738–1743.

32 L. X. Gao, Y. J. Wu, R. J. Li, J. L. Hai, X. F. Yue and Z. Y. Xie, Fabrication and electric-field response of spherical $BaTiO_3$ particles with high tetragonality, *J. Alloys Compd.*, 2015, **648**, 1017–1023.

33 S. Kango, S. Kalia, A. Celli, J. Njuguna, Y. Habibi and R. Kumar, Surface modification of inorganic nanoparticles for development of organic–inorganic nanocomposites - A review, *Prog. Polym. Sci.*, 2013, **38**, 1232–1261.

34 J. Su and J. Zhang, Remarkable enhancement of mechanical and dielectric properties of flexible ethylene propylene diene monomer (EPDM)/barium titanate ($BaTiO_3$) dielectric elastomer by chemical modification of particles, *RSC Adv.*, 2015, **5**, 78448–78456.

35 Y. P. Jiang, X. G. Li, S. R. Wang and Y. Xiao, Nano titanium dioxide particles modified with poly(lauryl methacrylate) and its electrorheological and electrophoretic behavior, *Colloids Surf., A*, 2014, **457**, 250–255.

36 D. Padalia, G. Bisht, U. C. Johri and K. Asokan, Fabrication and characterization of cerium doped barium titanate/PMMA nanocomposites, *Solid State Sci.*, 2013, **19**, 122–129.

37 L. P. Liu, Y. H. Zhang, F. Z. Lv, W. S. Tong, L. Ding, P. K. Chu and P. G. Li, Polyimide composites composed of covalently bonded $BaTiO_3$@GO hybrids with high dielectric constant and low dielectric loss, *RSC Adv.*, 2016, **6**, 86817–86823.

38 A. A. Thanki and R. K. Goyal, Study on effect of cubic- and tetragonal phased $BaTiO_3$ on the electrical and thermal properties of polymeric nanocomposites, *Mater. Chem. Phys.*, 2016, **183**, 447–456.

39 X. Zhang, S. Y. Wei, N. Haldolaarachchige, H. A. Colorado, Z. P. Luo, D. P. Young and Z. H. Guo, Magnetoresistive Conductive Polyaniline-Barium Titanate Nanocomposites with Negative Permittivity, *J. Phys. Chem. C*, 2012, **116**, 15731–15740.

40 L. Y. Xie, X. Y. Huang, C. Wu and P. K. Jiang, Core-shell structured poly(methyl methacrylate)/$BaTiO_3$ nanocomposites prepared by in situ atom transfer radical polymerization: a route to high dielectric constant materials with the inherent low loss of the base polymer, *J. Mater. Chem.*, 2011, **21**, 5897–5906.

41 S. Y. Oh and T. J. Kang, Electrorheological response of inorganic-coated multi-wall carbon nanotubes with core–shell nanostructure, *Soft Matter*, 2014, **10**, 3726–3737.

42 J. B. Yin, X. Xia and X. P. Zhao, Conductivity, polarization and electrorheological activity of polyaniline nanotubes during thermo-oxidative treatment, *Polym. Degrad. Stab.*, 2012, **97**, 2356–2363.

43 J. L. Chen, L. X. Gao, X. W. Han, T. Chen, J. Luo, K. Q. Liu, Z. W. Gao and W. Q. Zhang, Preparation and electro-response of chitosan-g-poly (acrylic acid) hydrogel elastomers with interpenetrating network, *Mater. Chem. Phys.*, 2016, **169**, 105–112.

44 J. B. Yin, X. P. Zhao, X. Xia, L. Q. Xiang and Y. P. Qiao, Electrorheological fluids based on nano-fibrous polyaniline, *Polymer*, 2008, **49**, 4413–4419.

45 L. X. Gao, J. L. Chen, X. W. Han, J. L. Zhang and S. X. Yan, Electric-field response behaviors of chitosan/barium titanate composite hydrogel elastomers, *J. Appl. Polym. Sci.*, 2015, **42094**, 1–6.

46 C. G. Niu, X. F. Dong and M. Qi, Enhanced Electrorheological Properties of Elastomers Containing TiO_2/Urea Core-Shell Particles, *ACS Appl. Mater. Interfaces*, 2015, **7**, 24855–24863.

47 N. Sakai, A. Fujishima, T. Watanabe, *et al.*, Enhancement of the photoinduced hydrophilic conversion rate of TiO_2 film electrode surfaces by anodic polarization, *J. Phys. Chem. B*, 2001, **105**(15), 3023–3026.

